Journal Name

Dynamic Article Links ►

Cite this: DOI: 10.1039/c0xx00000x

www.rsc.org/xxxxxx

ARTICLE TYPE

Synthesis of Binary Solid Solution Cu-Pd Nanoparticles by DMF Reduction for Enhanced Photoluminescent Properties

Masashi Chiba,[a] Mai Nguyen Thanh,[a] Yasuchika Hasegawa,[b] Yasushi Obora,[c] Hideya Kawasaki,[c] and Tetsu Yonezawa[a,*]

Received (in XXX, XXX) Xth XXXXXXXXX 20XX, Accepted Xth XXXXXXXXX 20XX
DOI: 10.1039/b000000x

We report use of a DMF reduction method for straightforward synthesis of binary solid solution Cu-Pd nanoparticles (NPs) over the entire range of composition. The resulting NPs were uniform in size (less than 2.5 nm), tunable in composition, and exhibited photoluminescent properties that were nonlinear in composition. These binary solid solution NPs exhibited values of such photoluminescent properties as photoluminescent intensity and quantum yield that were enhanced compared to those of the single-metal NPs and their mixtures. These enhancements make the alloy NPs promising materials for optical applications.

Introduction

Noble metal nanoparticles (NPs), such as Au, Ag, Cu, Pd and Pt, have attracted significant attention because, compared to bulk metals, they have unique and intriguing size-dependent properties. Optical, electrical and catalytic properties, as well as melting point depression, of metal NPs all depend on NP size, which makes them promising for applications such as optical devices, catalysis, biosensors, bioimaging and so on.[1-11] Moreover, in sizes of around 2 nm, metal NPs exhibit photoluminescent properties, which are otherwise dominated by semiconductor materials. Photoluminescent properties of metal NPs strongly depend on the size of the NPs, their surface condition, composition and the presence of stabilizing molecules. These parameters can be used to control and improve the photoluminescent property of metal NPs. Despite much effort, it remains difficult to precisely control the size of NPs in the range below 3 nm, which is the range needed for metal NPs to emit photoluminescence. However, properties of metal NPs can be tuned by doping and/or by alloying with other metals.[12-19] Therefore, creating alloy NPs with controllable composition should offer a feasible approach to modify the photoluminescent properties of noble metal NPs. While photoluminescent properties of noble metal NPs such as Au, Ag, Cu and Pd as well as some of their alloys, such as Au-Cu[14-15] or Au-Ag,[16-17] have been studied, little attention has been given to Cu and Pd solid solution NPs. At bulk scale, Cu and Pd can form binary solid solutions over the entire composition range, which makes them a good system for studying the formation and properties of binary metallic alloys at nanoscale. Therefore, our research is aimed at fabricating solid solution Cu-Pd NPs and investigating their photoluminescent properties as functions of alloy composition.

Various approaches have been reported for synthesizing photoluminescent metal NP dispersions, including chemical reduction, electrochemical deposition, laser ablation in liquid, matrix sputtering and so on.[20-23] Because of the ability to produce large quantities of NPs and the feasibility of controlling NP composition, size and structure, chemical reduction methods have been widely studied in terms of synthesis parameters, such as metal sources, reducing agents, solvents, stabilizing agents, temperature, etc. Many significant achievements in this research field have focused on utilizing different types of reducing agents to reduce the metal precursor and on various kinds of organic capping molecules for the soft template and stabilizing agent that control the formation of NPs. These approaches often require additional tasks to remove by-products and unreactive or excess compounds to obtain pure NP dispersions needed for investigations of their properties. Taking these considerations into account, many studies have focused on developing straightforward chemical syntheses that yield NPs without requiring subsequent separation or purification, especially for NPs in the cluster regime. Therefore, using N,N-dimethylformamide (DMF), which serves the triple role of solvent, reducing agent and stabilizing medium, is becoming one of the most potential approaches for synthesizing metal NPs in sizes below 3 nm.[25-29] The reducing power of DMF comes from the fact that, above 100 ^{o}C, DMF decomposes to carbon monoxide (CO) and dimethylamine, and the generated CO can reduce metal ions. At the same time, DMF can stabilize the resulting NPs without the addition of other stabilizing agents; this allows NP dispersion in DMF to be ready for use in studies of optical properties. Consequently, the DMF reduction method has been studied for synthesizing single-noble-metal NPs, such as Au, Ag, Pt, Pd and Cu.[26-29]

Therefore, we have used the DMF reduction method to produce solid solution Cu-Pd NPs in sizes that can produce photoluminescence. To study photoluminescent properties as functions of the composition of the binary solid solution NPs,

synthesized NPs must have similar sizes with high uniformity. Therefore, in our research, we focus on synthesis of solid solution Cu-Pd NPs with similar sizes and various compositions, and study their optical properties.

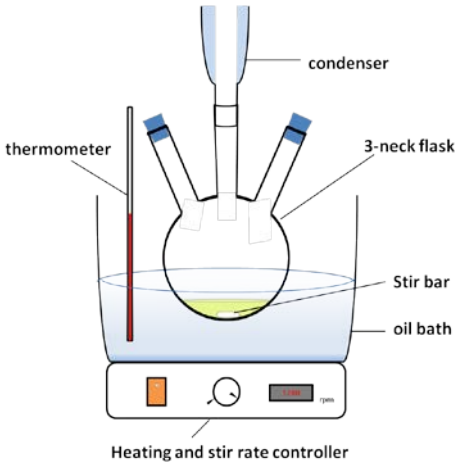

Figure 1. Experimental setup for synthesis of Cu-Pd NPs.

Experiment

Chemicals

N,*N*-dimethylformamide (DMF) (Wako, Japan) was used as the reducing agent and the protecting agent. The sources for metals were $CuCl_2$ (Kanto, Japan) and $PdCl_2$ (Kojima Chemical Co., Japan). Water was purified by an Organo/ELGA Purelabo system (resistivity > 18.2 kΩ) and used to prepare the metal ionic solutions.

Preparation of single-metal Cu, Pd, and binary solid solution Cu-Pd NPs

Prior to the synthesis of NPs, metal ionic solutions of Cu(II) and Pd(II) were prepared. $CuCl_2$ (134.6 mg) was dissolved in 10 mL of pure water to form a 0.1 M Cu(II) solution. A Pd(II) solution (0.1 M) was prepared by addition of 88.4 mg of $PdCl_2$ to 5 mL of DMF in a vial. To avoid the reduction of Pd(II), the vial was covered with aluminium foil. This solution was stirred for 24 h at room temperature to achieve a completely homogeneous dissolution of $PdCl_2$. Binary solid solution Cu-Pd NPs were synthesized according to the DMF reduction method given by Liu *et al*.[25] Briefly, 15 mL of DMF in a 50 mL three-neck round-bottom flask was heated to 140 °C while stirring at 1200 rpm in an oil bath. Then, the prepared Cu(II) solution was injected into the DMF followed by injection of Pd(II) solution (total metal ionic solution volume of 15 µL with volume ratios corresponding to the target composition) and heated at 140 °C while stirring at 1200 rpm for 16 h under ambient atmosphere (Figure 1). After that, the NP dispersions were allowed to naturally cool to room temperature and were used for further characterization. For single-metal NPs, 15 µL of only one of the metal sources was used in the synthesis.

Measurements and Characterization

Photoluminescent spectra, absolute quantum yields and UV-Vis spectra were measured using a photoluminescence spectrometer (JASCO FP-6600), JASCO F-6300-H spectrometer attached with a JASCO ILF-533 integrating sphere unit (ϕ=100 mm) and a UV-Vis spectrometer (JASCO V-630), respectively. UV-Vis spectra, photoluminescence spectra and quantum yields (QY) were measured for liquid samples using a quartz cell of 10 mm optical path.

The morphology and structures of NPs were observed using a transmission electron microscope (TEM) Hitachi H-9500 at an acceleration voltage of 300 kV, and a high-angle annular dark-field TEM JEOL JEM-ARM200F operated at 200 kV. Selected area electron diffraction (SAED) patterns were collected on a JEOL JEM-2010F with an acceleration voltage of 200 kV, and X-ray photoelectron spectra (XPS) were collected using a JEOL JPS-9200 with MgKα (1253.6 eV). Samples for TEM were prepared using an aliquot of ethanol-diluted (20 times) DMF dispersion dropped on a carbon-coated Cu grid and dried. NP sizes and size distribution histogram were calculated and plotted from 100 single NPs for each sample. Samples for SAED were prepared as follows: 3 mL of the DMF dispersion of NPs were concentrated at 35 °C under reduced pressure for 1 h, then they were diluted with 1 mL of ethanol and dropped on the TEM grid.

For XPS measurements, samples were prepared in the same way as samples for SAED. The same amounts of ethanol dispersions were dropped on silicon wafers (1 mm^2); the wafers had previously been immersed in a 1% HF solution for 1 h and cleaned in a UV-O_3 cleaner (Filgen) for 5 min. Then, the sample was heated to 60 °C to dry. The charging effect correction was applied using the binding energy of zero-valence Si $2p_{3/2}$ (99.2 eV) as the reference.

Results and discussion

Syntheses of solid solution Cu-Pd NPs with tunable compositions were conducted at input molar percentages of the precursors of 0%, 10%, 25%, 50%, 75%, 90% and 100% for each precursor. Figure 2 shows typical TEM images, SAED patterns and size distributions of the NPs prepared using input molar percentages of Cu to Pd (Cu/Pd) equal to (A) 100/0, (B) 50/50 and (C) 0/100 (see Supporting Information, Figure S1 for large view TEM images). From the TEM images, the average sizes of NPs were measured to be 2.0 ± 0.3, 2.3 ± 0.3, 1.8 ± 0.4 nm for the synthesis using only Cu, equimolar ratio of Cu and Pd, and only Pd precursors. Specific average sizes of NPs synthesized from different feeding ratios are given in Table 1. The table shows that, in all cases, NP sizes were about 2 nm (see Supporting Information, Figures S2-S5 for TEM images and size distributions of the NPs synthesized using other Cu/Pd feeding ratios). This similarity in NP sizes is critically important for our further investigations and comparisons of NP structures and optical properties.

The SAED patterns collected from these samples clearly indicated that the NPs had crystal structures. Moreover, the HAADF image of Cu-Pd NPs in Figure S5-B clearly shows the crystal structure for several single NPs. In Table 1, d-spacings calculated from the SAED patterns of the NPs are listed according to the feeding ratios used in the syntheses and the resulting NP sizes. Bulk Cu and Pd form binary solid solutions over the entire composition range and they all share the fcc structure. The d-spacings of the alloys depend on the composition of each metal component. The d-spacings corresponding to the

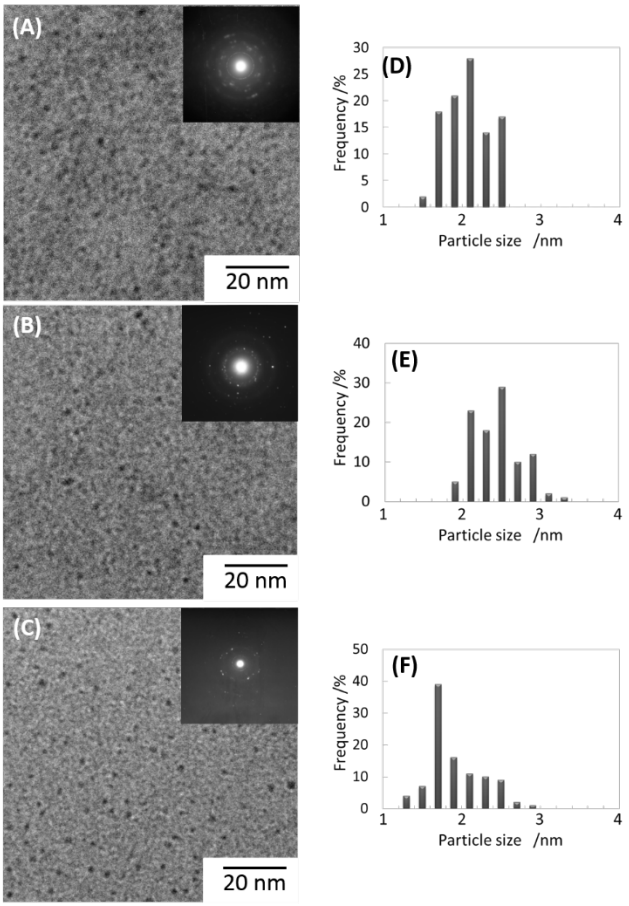

Figure 2. TEM images and size distributions of Cu NPs (A, D), Cu-Pd NPs synthesized using equimolar feeding ratio (B, E) and Pd NPs (C, F). Insets of TEM images are the corresponding SAED patterns for the NPs.

Table 1. d-Spacings of (111) crystal planes for as-synthesized NPs calculated from the SAED patterns

Feeding ratio (%)	Mean size (nm)	d-spacing of (111) plane (Å)	
		As-synthesized NPs	Reference (bulk alloy)[a,30]
Cu100Pd0	2.0±0.3	2.10	2.09
Cu90Pd10	2.3±0.5	NA	NA
Cu75Pd25	2.3±0.3	2.17	2.13
Cu50Pd50	2.3±0.3	2.18	2.18
Cu25Pd75	2.3±0.4	2.24	2.22 (Pd at. 78.4%)
Cu10Pd90	2.1±0.5	NA	NA
Cu0Pd100	1.8±0.4	2.32	2.25 2.30 (Pd 2.6 nm)[31] 2.29 (Pd 2.4 nm)[32] 2.35 (Pd 2 nm)[33]

[a]**The d-spacings of bulk Cu, Pd and alloys were calculated from the lattice parameter given in Reference 30**.

(111) crystal plane of the as-synthesized NPs increased as the Pd feeding ratios increased. The results in Table 1 show the same tendency as found in the bulk alloy with increasing Pd content.[30] This suggests the formation of binary solid solution Cu-Pd NPs

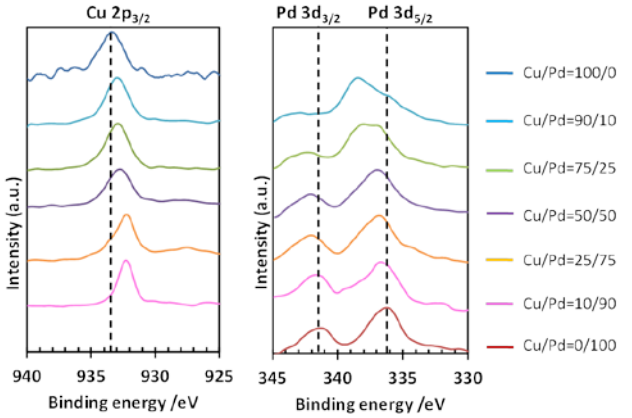

Figure 3. XPS core level spectra for Cu $2p_{3/2}$ and Pd 3d areas of Cu-Pd NPs with input feeding ratios for Pd increasing from top to bottom. Dashed lines mark the binding energy for (left) Cu $2p_{3/2}$ of Cu NPs (at 933.5 eV) and (right) Pd $3d_{5/2}$ and Pd $3d_{3/2}$ (336.2 and 341.4 eV, respectively) of Pd NPs.

and provides a good indication that the content of each component in the alloys is controlled by changing the feeding ratio of the precursors. Note that the d-spacings of the resulting NPs synthesized using all feeding ratios are slightly larger compared to the bulk counterparts. The most significant increase in d-spacing occurs for pure-metal Pd NPs, which have the smallest size (1.8 ± 0.4 nm) among all synthesized NPs (2.0 ± 0.3 nm for Cu NPs and 2.3 ± 0.3 for Cu-Pd NPs synthesized using an equimolar feeding ratio of Cu to Pd and so on). The Pd NPs in our experiment had a d-spacing of 2.32 Å for (111) planes while the corresponding value for bulk Pd is 2.25 Å. This different may be because of the large portion of surface atoms on Pd NPs since the Pd NPs were so small. As a result, the d-spacing increased, as shown in Table 1, especially for Pd NPs. This has been reported by other scientists for Pd NPs with even larger sizes; e.g. for 2.0–2.6 nm[31-33] the d-spacing was reported to be 2.29–2.35 Å compared to 2.25 Å of bulk Pd. Therefore, except for the pure-metal Pd and Cu NPs with smaller sizes, Cu-Pd NPs with similar sizes exhibited a systematic increase in d-spacing as the Pd feeding ratios was increased; this is a good evidence for the formation of binary solid solution NPs.

The formation of binary solid solution Cu-Pd NPs and the ability to control alloy compositions were further investigated using XPS spectra of Cu-Pd NPs. Figure 3 shows XPS core level spectra for Cu $2p_{3/2}$, Pd $3d_{5/2}$ and Pd $3d_{3/2}$ after correcting for charging effects using the zero-valence Si $2p_{3/2}$ peak at 99.2 eV and subtracting background.

In Figure 3, the binding energy positions for Cu $2p_{3/2}$ at 933.5 eV in Cu NPs, Pd $3d_{5/2}$ at 336.2 eV and Pd $3d_{3/2}$ at 341.4 eV in Pd NPs are marked by vertical dashed lines to aid the visualization of the chemical shifts. These values were higher than those of bulk Cu and Pd metals (Cu $2p_{3/2}$: 932.8 eV, Pd $3d_{3/2}$: 340.3 eV, Pd $3d_{5/2}$: 335.1 eV); these often originate from the reduction in screening of the core hole state by conduction electrons and the cores of neighbouring atoms during relaxation processes for metal NPs compared to those in bulk metals (cluster effect).[34-35] The screening effect seems to be stronger in Pd than in Cu, possibly because in a 3d transition metal like Cu, charge

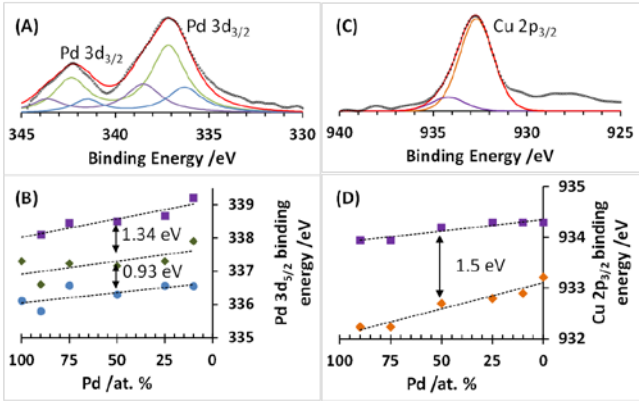

Figure 4. Peak deconvolutions for Pd 3d core level (A) and Cu 2p core level (C) in Cu-Pd NPs synthesized using the equimolar Cu/Pd feeding ratio. Red curve and dotted curve represent the sum of peak components and raw data, respectively. (B) and (D) give peak positions of each component of Pd $3d_{5/2}$ and Cu $2p_{3/2}$ as functions of Pd atomic feeding ratio, respectively.

screening partially comes from the less effective s electron, which is mostly negligible in Pd.

The core level spectra of Pd 3d contain peaks that are broad, highly asymmetric and even split at high Cu content; this may be due to the convolution of several Pd components. In our case, the Pd $3d_{5/2}$ spectrum can be deconvoluted into three symmetric peaks for Pd in Cu-Pd NPs and two for Pd single-metal NPs. These three components are assigned to PdO, the Pd core and the Pd surface in order of decreasing binding energy (Figure 4A); in Pd NPs, the PdO component seems negligible. The difference in the core level binding energy of the latter two components, Pd on the surface and Pd in the core of NPs, is mainly due to the smaller amount of bonding of Pd that can occur on NP surfaces. Hetero-bonding of Pd with Cu may mainly cause the core binding energy of Pd to be positively shifted (explained below). The binding energy separation between the first and second components is in good agreement with that between PdO and zero-valence Pd for the bulk metal. For the Cu 2p core level, curve fitting can be done using two components in which the first component at the higher binding energy belongs to copper oxide (CuO) and the other is for zero-valence Cu (Figure 4C). The oxide component is most significant in single-metal Cu and quickly decreases as the Pd feeding ratio increases; this behaviour is opposite to that of the relative intensity of the oxide component in the Pd 3d core level (data not shown). Details of the peak parameters are given in the Supporting Information.

Figure 4B shows the XPS 3d core level of Pd in the Cu-Pd NPs, and the relation of each component to the feeding ratio of Pd. The most positive shifts in all Pd components occurred for NPs synthesized with low Pd ratios because there is increased possibility that relatively small amounts of Pd will be better distributed in a Cu matrix. For Cu $2p_{3/2}$, the most negative shift appeared in Cu-Pd NPs synthesized using high feeding ratios of Pd (Figure 4D). Considering core level peak positions for Cu-Pd NPs over the entire range of composition, Cu $3p_{3/2}$ shifts to lower binding energies as the Pd ratio increased, while Pd $3d_{5/2}$ (both core and surface components) shifts to higher binding energies as

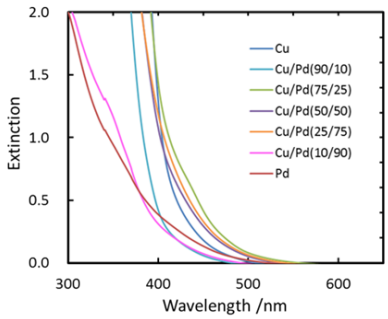

Figure 5. UV-Vis extinction spectra of as-synthesized Cu-Pd NPs with various molar feeding ratios.

the Cu ratio increased. This is similar to what has been observed for the bulk Cu-Pd alloy.[36] This is explained based on the formation of Cu-Pd alloy, which can modify the electronic structure of the valence d band of both Cu and Pd in such a way that the electron density near the Fermi level in Cu increases with an opposite change in valence band for Pd. In transition metals, screening of the core hole by d electrons is most effective, so the electron density in the valence band strongly affects relaxation of the core hole. As a result, increasing Cu content in the Cu-Pd alloy increases the positive shift of Pd $3d_{5/2}$ while the opposite occurs for Cu $2p_{3/2}$.[36] The shift of core level binding energies for Cu and Pd in Cu-Pd NPs with composition further contributed to the formation of the binary solid solution Cu-Pd NPs. In addition to the analysis of SAED shown previously, these results for XPS indicated the successful formation of binary solid solution Cu-Pd NPs by the DMF reduction method. Even though elemental analysis for single or several NPs is not feasible using TEM-EDS, due to the fact that very small NPs capped with organic molecules cause low signals of Cu and Pd, and hardly clearly distinguish from the background, successful alloy formation and the later confirmation of complete reaction (UV-Vis results) of precursors suggest that composition of NPs are as same as the corresponding feeding ratios.

Optical properties

Optical properties of the synthesized NPs were investigated using UV-Vis and photoluminescent spectroscopy. Figure 5 shows UV-Vis extinction spectra for our solid solution Cu-Pd NPs. The absence of absorption for $PdCl_2$ and $CuCl_2$ indicates that the precursors were completely consumed in the reaction. Absorption edge locations shift to longer wavelengths as the amounts of the two metals approach each other, and the location reaches the longest wavelength for the sample synthesized using the equimolar ratio of Cu to Pd. The change in the absorption edge with composition of NPs may arise from the change in the energy gap of the resulting solid solution NPs due to alloying between Cu and Pd. In the bulk dilute Cu-Pd alloy, alloying increases the electron density near the Fermi level of the Cu-d band for Cu-rich alloy as the amount of Pd increases. In contrast, adding Cu to Pd-rich alloy causes some withdrawal of electron density near the Fermi level of the Pd d-band. Therefore, the strength of the effect that each metal has on the other when alloying and their amounts in the alloy determine the energy gap of alloy NPs, especially when the amounts of both metals are not negligible. In this case, the Cu-Pd NPs synthesized from

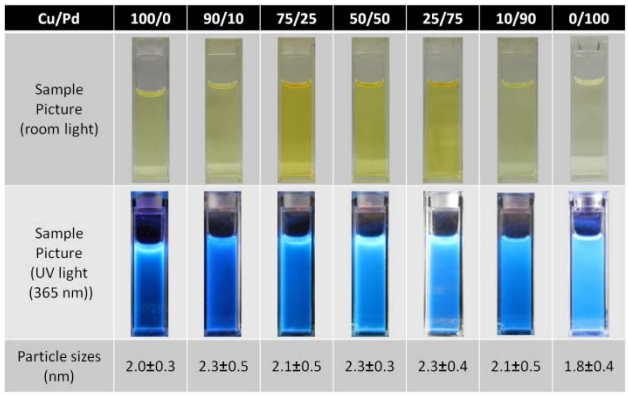

Figure 6. Photograph of Cu-Pd alloy NPs for various molar feeding ratios under room light (upper row) and under UV light of 365 nm (lower row).

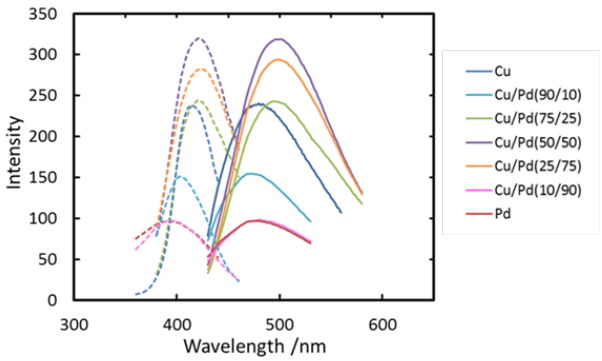

Figure 7. Photoluminescent spectra with the excitation spectra (dashed lines) and emission spectra (solid lines) of as-synthesized Cu-Pd NPs for various molar feeding ratios.

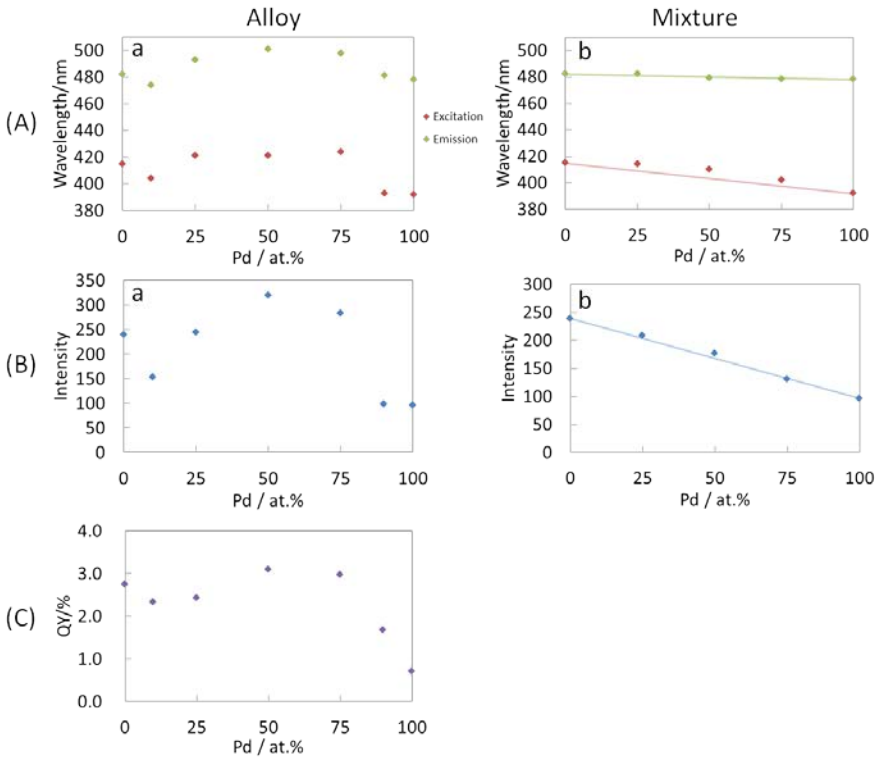

Figure 8. Photoluminescence peak position (A), intensity (B) and quantum yield (C) of solid solution Cu-Pd NPs (left column) and corresponding values for mixtures of single-metal Cu and single-metal Pd NPs (right column). Dots in panels (A-b) and (B-b) were obtained from mixture of single-metal Cu and Pd NPs; lines connecting pure Cu and pure Pd NPs are to guide the eye.

equimolar feeding ratio had the smallest energy gap; this may be because of the largest rise in the valence band of alloy NPs, which is a result of strong hybridization of Cu and Pd d-band occur at the equimolar composition.[35]

The resulting NPs have the photoluminescent properties shown in Figures 6 and 7. Figure 6 shows photographs of Cu-Pd dispersions under room light and UV light (365 nm); in the later, the samples clearly emit blue photoluminescence. Figure 7 compares excitation and emission spectra of Cu-Pd NPs for various Cu/Pd feeding ratios. The excitation wavelength, emission wavelength and photoluminescence intensity change with composition. Moreover, the sample with the least amount of Pd was excited by and emitted shorter wavelengths, while samples containing close to equimolar amounts of Cu and Pd show the longest wavelength emissions. This is consistent with the UV-Vis absorption results. To analyse the relation between photoluminescent properties and alloy NP composition, not only the photoluminescent peak position but also the peak intensity and quantum yield are plotted versus feeding ratios (Pd atomic %) in Figure 8. Corresponding values for mixtures of Pd and Cu NPs are also included for comparison. Figure 8(A-a) shows how the peak position of alloy NPs changes with

composition, while Figure 8(A-b) does the same for mixtures of single-metal Cu and single-metal Pd NPs. Figure 8(B) shows the effects of composition on peak intensities of alloy samples and mixtures of single-metal NPs. Nearly linear changes occurred for mixtures of single-metal NPs, while synthesized alloy NPs show nonlinear relations between feeding ratios and photoluminescent peak position, photoluminescent intensity and absolute quantum yield. In each case, the maximum occurred at the equimolar feeding ratios. For photoluminescent intensity, the maximum at equimolar ratio, probably occurred because enhancement of electron density in the Cu d-band was largest at that composition, and this electron density is main contributor to photoluminescent emission.

Similar to the trends in excitation wavelength, emission wavelength and photoluminescence intensity, solid solution Cu-Pd NPs show enhanced quantum yield, especially compared to the single-metal NPs (2.75% for Cu NPs and 0.71% for Pd NPs). The sample obtained from the equimolar feeding ratio had the highest quantum yield (3.10%). These results indicate that Cu-Pd NPs with higher photoluminescence intensity and quantum yields can be synthesized using DMF reduction. In contrast, in Au-Cu alloy NPs, the properties were bounded by the values for single-metal NPs.[14] In Cu-Pd alloy NPs, photoluminescent properties were enhanced compared to those in the corresponding single-metal NPs. This result is important for alloy NPs to modify and improve photoluminescent properties.

Conclusions

Binary solid solution Cu-Pd NPs with uniform sizes and tunable composition have been successfully synthesized using a DMF reduction method. The resulting alloy NPs show enhanced photoluminescent properties compared to single-metal NPs with similar sizes. Even though the origins of the enhancements are still under investigation, the formation of solid solution Cu-Pd NPs has been demonstrated to be a straightforward way to control and improve the photoluminescent properties of metal NPs, so this synthesis method is promising for various optical applications.

The authors thank to Drs. S. Maenosono and K. Higashimine in JAIST for taking HAADF images of our sample.

Notes and references

[a] *Division of Materials Science and Engineering, Faculty of Engineering, Hokkaido University, Kita 13 Nishi 8, Sapporo, Hokkaido 060-8628, Japan. *E-mail: tetsu@eng.hokudai.ac.jp*

[b] *Division of Chemistry, Faculty of Engineering, Hokkaido University, Kita 13 Nishi 8, Kita-ku, Sapporo, Hokkaido 060-8628, Japan*

[b] *Department of Chemistry, Kansai University, Yamate-cho, Suita-shi, Osaka, Japan*

† Electronic Supplementary Information (ESI) available: [TEM, HAADF-STEM images and size distribution of Cu-Pd nanopartilces synthesized using different molar feeding ratios, and curve fitting parameters of XPS core level spectra of Cu 2p and Pd 3d]. See DOI: 10.1039/b000000x/

‡ Footnotes should appear here. These might include comments relevant to but not central to the matter under discussion, limited experimental and spectral data, and crystallographic data.

1 J. Zheng, P. R. Nicovich, and R. M. Dickson, *Annu. Rev. Phys. Chem.*, 2007, **58**, 409.

2 X. Yuan, Z. Luo, Q. Zhang, X. Zhang, Y. Zheng, J. Y. Lee, and J. Xie, *ACS NANO*, 2011, **5**, 8800.

3 Y. Lee, J. Choi, K. J. Lee, N. E Stott, and D. Kim, *Nanotech.*, 2008, **19**, 415604.

4 Y. Kobayashi, T. Shirochi, Y. Yasuda, and T. Morita, *Solid State Sci.*, 2011, **13**, 553-558.

5 O. M. Wilson, M. R. Knecht, J. C. Garcia-Martinez, and R. M. Crooks, *J. Am. Chem. Soc.*, 2006, **128**, 4510.

6 A. C. Atesin, N. A. Ray, P. C. Stair, and T. J. Marks, *J. Am. Chem. Soc.*, 2012, **134**, 14682.

7 A. D. McFarland, and R. P. V. Duyne, *Nano Lett.*, 2003, **3**, 1057.

8 N. Toshima, and T. Yonezawa, *New J. Chem.*, 1998, **22**, 1179.

9 N. Toshima, K. Kushihashi, T. Yonezawa, and H. Hirai, *Chem. Lett.*, 1989, **18**, 1769.

10 N. Toshima, T. Yonezawa, M. Harada, K. Asakura, and Y. Iwasawa, *Chem. Lett.*, 1990, **19**, 815.

11 Y. Y. Tong, T. Yonezawa, N. Toshima, and J. J. van der Klink, *J. Phys. Chem.*, 1996, **100**, 730.

12 Y. Negishi, K Munakata, W. Ohgake, and K Nobusada, *J. Phys. Chem. Lett.*, 2012, **3**, 2209.

13 W. Kurashige, K. Munakata, K. Nobusada, and Y. Negishi, *Chem. Commun.*, 2013, **49**, 5447.

14 C. M. Andolina, A. C. Dewar, A. M. Smith, L. E. Marbella, M. J. Hartmann, and J. E. Millstone, *J. Am. Chem. Soc.*, 2013, **135**, 5266.

15 P. C. Chen, J. Y. Ma, L. Y. Chen, G. L. Lin, C. C. Shih, T. Y. Lin, and H. T. Chang, *Nanoscale*, 2014, **6**, 3503.

16 B. Paramanik, and A. Patra, *J. Mater. Chem. C.*, 2014, **2**, 3005.

17 M. Chen, Z. Lei, W. Feng, C. Li, Q. M. Wang, and F. Li, *Biomaterials*, 2013, **34**, 4284.

18 X. Gu, Z.-H. Lu, H.-L. Jiang, T. Akita, and Q. Xu, *J. Am. Chem. Soc.*, 2011, **133**, 11822.

19 S. Zhang, Ö. Metin, D. Su, and S. Sun, *Angrew. Chem. Int. Ed.*, 2013, **52**, 3681.

20 M. Ganguly, A. Pal, Y. Negishi, and T. Pal, *Chem. Eur. J.*, 2012, **18**, 15845.

21 H. Zhang, X. Huang, L. Li, G. Zhang, I. Hussain, Z. Li, and B. Tan, *Chem. Commun.*, 2012, **48**, 567.

22 N. Vilar-Vidal, M. C. Blanco, M. A. Lopez-Quintela, J. Rivas, and Carmen Serra, *J. Phys. Chem. C*, 2010, **114**, 15924.

23 M. Muniz-Miranda, C. Gellini, and E. Giorgetti, *J. Phys. Chem. C*, 2011, **115**, 5021.

24 K. Nakagawa, T. Narushima, S. Udagawa, and T. Yonezawa, *J. Phys. Conf. Ser.*, 2013, **417**, 012038.

25 X. Liu, C. Li, J. Xu, J. Lv, M. Zhu, Y. Guo, S. Cui, H. Liu, S Wang, and Y. Li, *J. Phys. Chem. C*, 2008, **112**, 10778.

26 H. Kawasaki, H. Yamamoto, H. Fujimori, R. Arakawa, Y. Iwasaki, and M. Inada, *Langmuir*, 2012, **26**, 5926.

27 H. Kawasaki, H. Yamamoto, H. Fujimori, R. Arakawa, M. Inada, and Y. Iwasaki, *Chem. Commun.*, 2010, **46**, 3759.

28 M. Hyotanishi, Y. Isomura, H. Yamamoto, H. Kawasaki, and Y. Obora, *Chem. Commun.*, 2011, **47**, 5750.

29 Y. Isomura, T. Narushima, H. Kawasaki, T. Yonezawa, and Y Obora, *Chem. Commun.*, 2012, **48**, 3784.

30 P. R. Subramanian, and D. E. Laughlin, *J. Phase Equilib.*, 1991, **12**, 231.

31 M. Yamauchi, and H. Kitagawa, *Synthetic Met.*, 2005, **153**, 355.

32 T. Teranishi, and M. Miyake, *Chem. Mater.*, 1998, **10**, 594.

33 J. W. M. Jacobs, and D. Schryvers, *J. Catal.*, 1987, **103**, 436.

34 M. G. Mason, *Phys. Rev. B*, 1983, **27**, 748.

35 G. K. Wertheim, S. B. DiCenzo, and D. N. E. Buchanan, *Phys. Rev. B*, 1986, **33**, 5384.

36 N. Martensson, R. Nyholm, H. Calen, J. Hedman, and J. Johansson, *Phys. Rev. B*, 1981, **24**, 1725.